

# Plasmonic Thermal Emitters for Dynamically Tunable Infrared Radiation

Amir Kazemi Moridani, Robert Zando, Wanting Xie, Irene Howell, James J. Watkins, and Jae-Hwang Lee\*

Periodic bimetallic microstructures using nickel and gold are fabricated on an elastomeric substrate by use of strain-induced buckling of the metallic layers, which can be compatible with roll-to-roll manufacturing. The intrinsically low emissivity of gold in the midinfrared regime is selectively enhanced by the surface plasmonic resonance at three different midinfrared wavelengths, 4.5, 6.3, and 9.4  $\mu\text{m}$ , respectively, which directly correspond to the structural periodicities of the metallic microstructures. As the thermal emission enhancement effect exists only for the polarization perpendicular to the orientation of the microstructures, substantially polarized thermal emission with an extinction ratio close to 3 is demonstrated. Moreover, the elastically deformed plasmonic thermal emitters demonstrate strain-dependent emission peaks, which can be applied for future mechano-thermal sensing and dynamic thermal signature modulation.

Thermal radiation of an object is the universal energy transport via thermally emitted photons. Its photon energy spectrum is governed by the object's temperature and emissivity spectrum,  $\epsilon(\lambda)$ . Since a dominant radiation wavelength range of the photons typically falls within the micro- or sub-micrometer scales,  $\epsilon(\lambda)$  can be systematically modified by physical microstructuring of radiating material's surface at a scale comparable to the wavelengths. As a result, several engineered microstructures have demonstrated modified thermal radiation.<sup>[1,2]</sup> Among the microstructures, periodic metallic structures have been known to be able to selectively enhance thermal radiation in a specific range of infrared wavelengths due to altered density of states of surface plasmons, quanta of collective vibration modes of free electrons at the metallic surface adjacent to a dielectric medium.<sup>[3–9]</sup> In addition to the spectral modification of thermal radiation, since angular distribution<sup>[10,11]</sup> and polarization<sup>[12–14]</sup> can also be engineered, new opportunities

in thermal radiation management have been envisioned, for examples, thermal stealth,<sup>[15,16]</sup> passive radiative cooling,<sup>[17,18]</sup> energy conversion,<sup>[14,19]</sup> and sensing.<sup>[20,21]</sup>


Since engineered thermal radiative characteristics are directly correlated to the geometrical parameters of the periodic structures, mechanical deformation of the periodic structures is conceptually straightforward to realize dynamically tunable thermal emitters. However, due to the mechanical and optical stabilities of material platforms, only the control of materials' optical parameters through an electrical charge injection has been recently demonstrated.<sup>[22]</sup> For the midinfrared (mid-IR) range (3–10  $\mu\text{m}$ ), because the desired working temperatures can be below 300 °C, crosslinked elastomers such

as silicone can be considered as a deformable material platform to achieve dynamically tunable thermal emitters. Here, we report deformable plasmonic thermal emitters (PTEs) using a hybrid material platform that is applicable for mechanically tunable polarized thermal emission. Moreover, as the functional periodic structures are spontaneously created by strain-induced folding,<sup>[23–25]</sup> the demonstrated fabrication method can be compatible with roll-to-roll manufacturing process for scale-up production. These characteristics, combined with the high elastic characteristics of commercial elastomers ( $\approx 200\%$  tensile deformation), allow for the production of devices with a wide range of potential spectral emission enhancement capabilities within the mid-IR wavelength region. For example, we envision that the demonstrated PTE structures can be applied to strain-based sensor patches, which can be operated by human body heat.

All PTEs were fabricated based on the idea of structure formation in metallic films on an elastomeric substrate. First, a 1.5 mm thick substrate of polydimethylsiloxane (PDMS) was prepared by mixing a 10:1 ratio of silicone elastomer resin and curing agent (Sylgard 184, Dow Corning) and curing at 125 °C for 1 h. After curing, nickel was deposited on the uniaxially stretched PDMS substrate and regularly periodic wrinkle patterns were spontaneously formed along the direction perpendicular to the stretching direction because of buckling instability when the PDMS substrate was relaxed to its original dimensions. The periodicity of the wrinkle pattern was controlled by the deposition thickness of the nickel film. Three different periodicities ( $\Lambda$ ), 4.5, 6.3, and 9.4  $\mu\text{m}$ , were fabricated for studying their thermal emission. Based on Equation (1),<sup>[26]</sup>

A. Kazemi Moridani, R. Zando, W. Xie, Prof. J.-H. Lee  
Department of Mechanical and Industrial Engineering  
University of Massachusetts  
Amherst, MA 01003, USA  
E-mail: leejh@umass.edu

I. Howell, Prof. J. J. Watkins  
Department of Polymer Science and Engineering  
University of Massachusetts  
Amherst, MA 01003, USA

 The ORCID identification number(s) for the author(s) of this article can be found under <http://dx.doi.org/10.1002/adom.201600993>.

DOI: 10.1002/adom.201600993

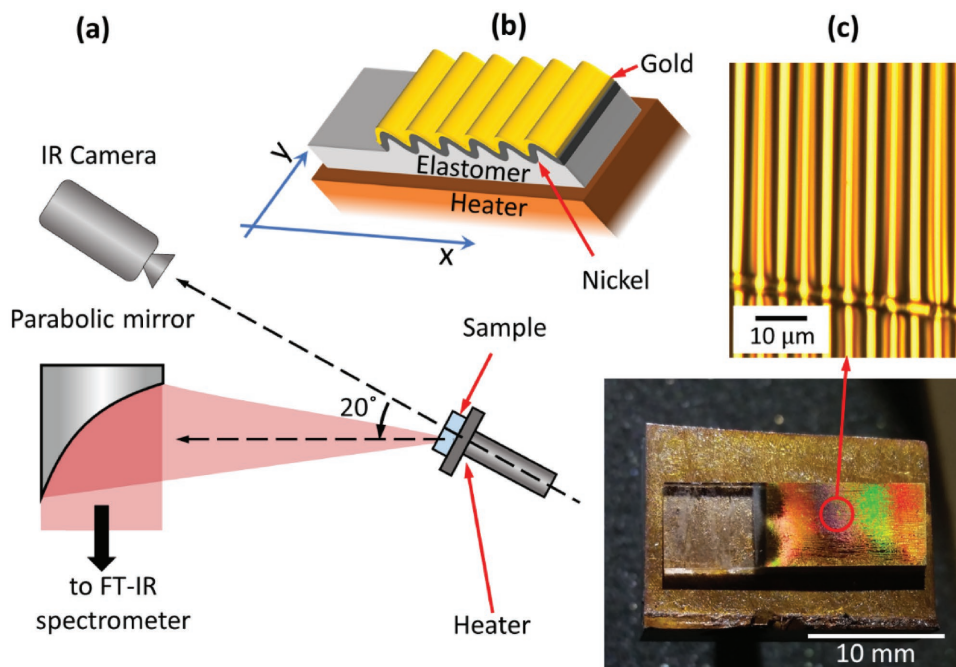


**Figure 1.** a) Schematic illustration of the radiometric experiment setup. b) Structure of the samples. c) Optical images of the sample on a heater surface.

the corresponding thicknesses ( $d$ ) of the nickel films were estimated to be 25, 35, and 52 nm using elastic moduli of nickel and PDMS,  $E_f$  and  $E_s$ , and Poisson's ratios of nickel and PDMS,  $\nu_f$  and  $\nu_s$

$$\Lambda = 2\pi d \left[ \frac{(1-\nu_s^2)E_f}{3(1-\nu_f^2)E_s} \right]^{1/3} \quad (1)$$

In order to have the intrinsically low emissivity in mid-IR, the nickel-coated structure was coated with another 50 nm thick layer of gold after the wrinkles were formed. Note that the approach using two different metals, gold and nickel, provides better design capability to optimize each material for optical or structural need independently. Measurements were made using a Fourier transform (FT) IR spectrometer (Nicolet 6700, Thermo Scientific) with an external IR optics for mid-IR radiometry (Figure 1a).<sup>[12]</sup> A mercury cadmium telluride (MCT)-A detector with liquid nitrogen cooling was used to measure near-room-temperature IR radiation. The radiometric setup was calibrated using a lab-built blackbody source. For quantitative radiometric characterization, total IR radiation flux was limited to ensure the detector's linear response.<sup>[27]</sup> The radiometry setup showed less than 1% error in measuring blackbody radiation.

The temperature of the samples was controlled by an electrical heater using a copper plate to ensure a uniform temperature distribution across the samples. As shown in Figure 1b,c, the left region of the elastomer was not coated with the metallic layers and this uncoated region was used as a reference material to define the surface temperature of the sample as measured by a calibrated mid-IR camera (T450sc, FLIR). The thick layer of PDMS ( $\approx 1.5$  mm) shows less than 0.1% transmission for the spectral range of the camera (7.5–13 μm); making

PDMS a good reference material for the temperature definition using the mid-IR camera.<sup>[28–30]</sup> To exclude the thermal radiation from the FT-IR radiometer itself, which was reflected at PTE's surface, all thermal radiation measurements were performed at a tilted angle of 20° about the x-axis with respect to the optical axis of the IR collecting optics. In addition, any temperature-independent radiation signals were also excluded by comparing the radiation spectra at two different temperatures, 75 and 90 °C. The measured radiation spectra were converted to corresponding  $\epsilon(\lambda)$  by normalization to that of blackbody and this gives averaged  $\epsilon(\lambda)$  within these two temperatures.

The PTEs had a regular sinusoidal height profile as shown in Figure 2a. Since the periodic structures were created by the buckling instability when a stretched PDMS substrate (up to 20% strain) was released, the lateral deformation by the positive Poisson's ratio of PDMS created unintended cracks perpendicular to the orientation of the periodic structures in the nickel layer, as seen in the scanning electron microscope (SEM) image. Quantitative height profiles of the different structures were measured by an optical profilometer (Nexview, Zygo) as shown in Figure 2b–d. The density of the cracks was typically on the order of 10 cracks per 1 mm, which is significantly smaller than the periodicities of the structures. With the exception of these cracks, all the structures were very regular. For all the samples, the peak-to-peak amplitude of each periodic structure was  $\approx 20\%$  of its periodicity.

The measured emissivity spectra are shown in Figure 3 for two principal polarization angles, parallel ( $\parallel$ , along the y-axis) and perpendicular ( $\perp$ , along the x-axis) to the orientation of the periodic structure. All thermal emissions are highly polarized and only  $\epsilon_{\perp}(\lambda)$  demonstrates the emission peak arising from the fundamental plasmonic resonance modes at the wavelength close to the periodicity of each structure. Note that the

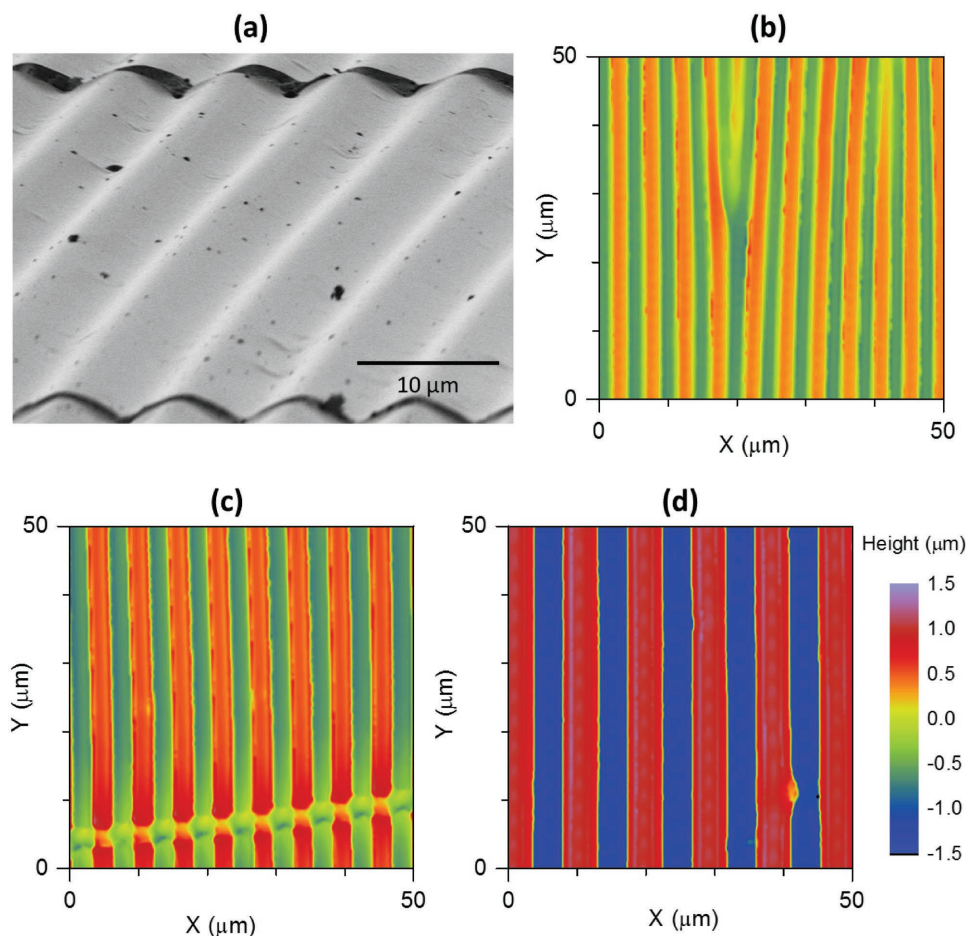


**Figure 2.** Height profiles PTEs. a) SEM image of a PTE at a tilt angle of 85°. Vertical profiles of PTEs having three different periodicities, b) 4.5 c) 6.3, and d) 9.4  $\mu\text{m}$ , respectively with the common vertical scale.

fluctuating features of the spectra below 3.5  $\mu\text{m}$  were due to a low signal to noise ratio arising from weak radiation signal and low sensitivity of the MCT-A detector within the spectral range. The 9.4  $\mu\text{m}$  structure also exhibits an additional emission peak ( $\lambda = 4.42 \mu\text{m}$ ) from the higher order resonance in the measured mid-IR range, which can be explained by the surface plasmon band structures of metallic gratings.<sup>[31]</sup> In contrast,  $\epsilon_{\parallel}(\lambda)$  was almost constant and low for all of the PTEs. The

extinction ratio  $\left(\frac{\epsilon_{\perp}}{\epsilon_{\parallel}}\right)$ , which is defined by the ratio between

two emissivity spectra of two polarizations to show the relative radiation power in the two perpendicular polarizations, is also shown in Figure 3. All the PTEs showed a large extinction ratio at the resonance wavelengths, which is very useful for mid-IR applications utilizing polarized thermal emission. The maximum emissivity was higher for a narrower specific width of the emission peak ( $\Delta\lambda/\lambda$ ). We believe that this trend can be explained by the regularity of the periodic patterns because the thermal radiation power from each local emitting element can be concentrated within a narrower range of wavelengths, which leads to the higher emissivity. The 9.4  $\mu\text{m}$  periodicity structure showed a distorted emission peak in the range of 8–10  $\mu\text{m}$  and

$\epsilon_{\parallel}$  also showed an unexpected radiative feature that should not be created by gold. As shown in Figure 3d, these unusual features correspond to the strong molecular absorption feature of PDMS. The IR transmission spectrum of the samples in Figure 3d was very low ( $<0.2\%$ ) and increased up to 1.5% in the shorter wavelength region. If considering the thick deposition of nickel–gold bilayer, the transmittance spectrum has to be explained by the limited optical transmission through some open cracks on the metallic layer (Figure 2 a, c). Therefore, we believe that the unusual emission signature could primarily be a result of direct transmission of thermal emission of the PDMS substrate through some open cracks, which can be wider at the elevated temperatures due to thermal expansion of PDMS. We also note that the emission feature originating from the molecular resonance of PDMS can be transmitted via the indirect plasmonic coupling through the nickel–gold bilayer as observed in surface plasmonic absorption.<sup>[32–35]</sup>

Results of the strain-dependent radiation measurements for the perpendicular polarization are shown in Figure 4 for five different uniaxial tensile strain values up to 12.8%. The peak position of  $\epsilon_{\perp}(\lambda)$  was shifted toward longer wavelength due to the increasing structural periodicity corresponding to the tensile deformation. Figure 4b shows that the peak position shift was

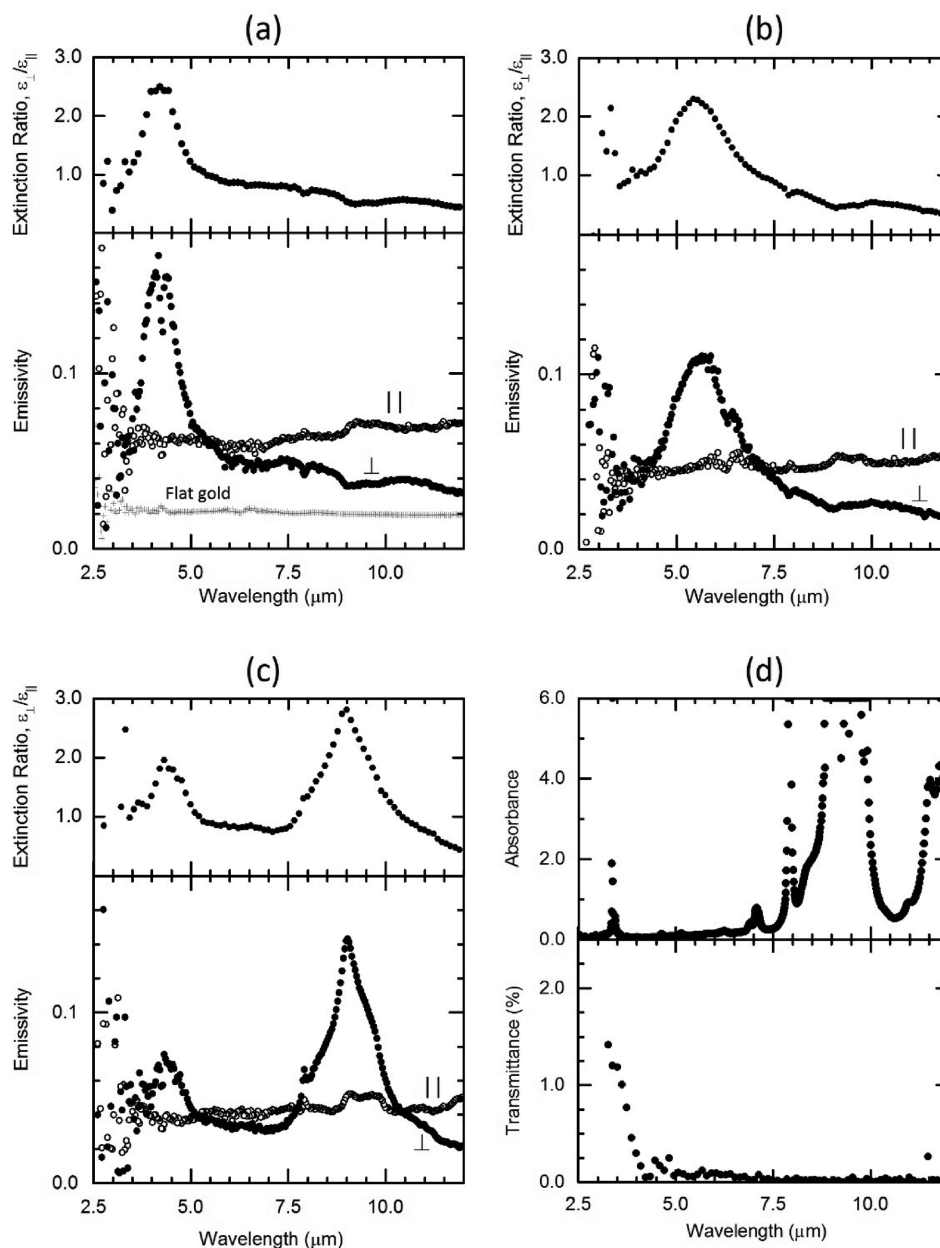


**Figure 3.** Polarization-dependent thermal radiative characteristics, emissivity, and extinction ratio of the samples having three different periodicities, a) 4.5, b) 6.3, and c) 9.4 μm. d) Absorbance of a 26 μm thick PDMS-only substrate (top) and typical IR transmittance of the PDMS substrate with a periodic metallic structure (bottom).

linearly proportional to the strain. In addition to the redshift of the peak position, the peak emissivity was also considerably reduced as strain increases. Since the plasmonic structure was created by the contraction of the PDMS substrate, the applied tensile strain therefore returned the wrinkled metallic film to close to its original flat state, i.e., the structural amplitude of the wrinkles was decreased. As the PTE structure has a microscopically wrinkled surface, we ought to consider an effective radiation surface,  $A_{\text{eff}}$ , increasing for a larger structural amplitude of the wrinkle depending on the applied tensile strain. Consequently, a larger tensile strain reducing  $A_{\text{eff}}$  resulted in a lower emissivity. With the exception of the  $A_{\text{eff}}$  effect, however, the variation in

the structural amplitude may also affect the dynamics of plasmonic resonance. Figure 4c shows emissivity ratios defined by  $\epsilon_{\perp}(\lambda)$  of PTE and flat gold at the two different wavelengths, resonance peak, and resonance edge ( $\lambda = 10.5$  μm). Again, regardless of strains, all emissivity spectra of PTE were higher than that of a flat gold surface primarily due to the increased  $A_{\text{eff}}$ . In the semilog plot, as the two ratios show a very similar trend, this suggests that the change in structural amplitude does not alter the dynamics of plasmonic resonance. Regarding structural stability under repeated tensile deformation, the demonstrated PTE structures were stable for less than ten cycles of tensile deformation. The deterioration of the PTE structure under

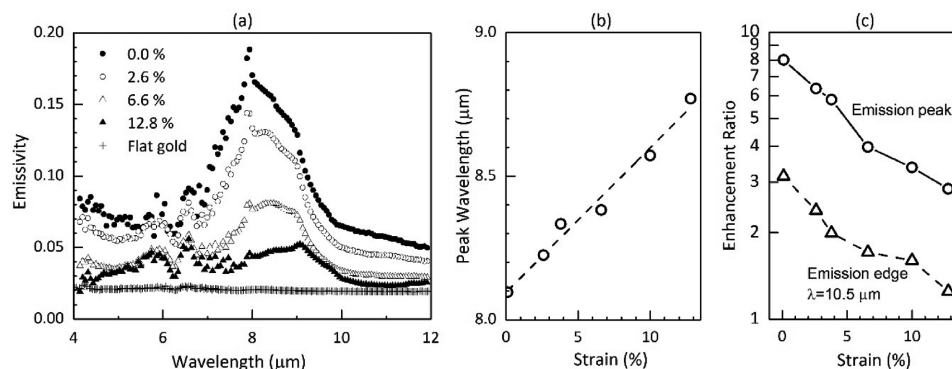


**Figure 4.** Strain-induced spectral changes. a) Emissivity at different strains, the features transmitted through open cracks and plasmon-mediated coupling are visible as a spike at 7.9 μm and two kinks at ≈9–10 μm. The oscillatory feature at 5.5–7 μm regions are originating from the molecular absorption bands of water vapor in air. b) Change in the peak position versus strain. c) Semilog plot of emissivity enhancement ratios at the emission peak and emission edge wavelengths.

the cyclic stresses was mainly due to the insufficient adhesion of nickel to PDMS. We expect that the structural stability can be improved by replacing nickel with chromium, a stiff metal known for better adhesion to PDMS.<sup>[36,37]</sup>

In conclusion, engineering of mid-IR thermal radiation characteristics was demonstrated with periodic metallic microstructures, created on elastomeric substrates without using any top-down patterning tools. Plasmonic thermal emission was depending on the structure's periodicity and orientation. The deformable PTEs can be utilized for mechano-thermal strain sensors, simultaneously monitoring strain and orientation. Moreover, we were able to demonstrate the dynamic modulation of thermal signature of the deformable plasmonic structures, which is potentially advantageous in defense applications. Certainly, various lithographical techniques are also available for patterning periodic elastomer structures, which will allow for more diverse functional plasmonic emitters. For instance, the dependency of the structural amplitude on the strain can be reduced by using prepatterned elastomer substrates, which will result in almost the same degree of enhancement while changing the periodicity. For wide-area plasmonic thermal emitters, aluminum can be considered as a low-cost and industry-friendly alternative material of gold because aluminum structures also demonstrated sufficient plasmonic resonances in the recent studies.<sup>[38,39]</sup> The dynamic mechanical deformation can induce crack formation or delamination of the metallic layer from the elastomeric substrates. However, we envision that the introduction of mechanical metamaterials having near-zero Poisson's ratio and interfacial engineering between an elastomer and a metallic layer will alleviate these technical issues.

## Acknowledgements

This work was supported by the NSF Center for Hierarchical Manufacturing at the University of Massachusetts (CMMI-1025020).

## Conflict of Interest

The authors declare no conflict of interest.

## Keywords

dynamic tuning, thermal stealth, metamaterials, plasmonic resonances, thermal signatures

Received: November 28, 2016

Revised: February 24, 2017

Published online: April 7, 2017

- [1] V. Rinnerbauer, S. Ndao, Y. X. Yeng, W. R. Chan, J. J. Senkevich, J. D. Joannopoulos, M. Soljacic, I. Celanovic, *Energy Environ. Sci.* **2012**, 5, 8815.
- [2] M. M. Hossain, M. Gu, *Adv. Sci.* **2016**, 3, 1500360.
- [3] H. Sai, Y. Kanamori, H. Yugami, *Appl. Phys. Lett.* **2003**, 82, 1685.
- [4] H. Sai, Y. Kanamori, H. Yugami, *J. Micromech. Microeng.* **2005**, 15, S243.
- [5] M. W. Tsai, T. H. Chuang, C. Y. Meng, Y. T. Chang, S. C. Lee, *Appl. Phys. Lett.* **2006**, 89, 173116.
- [6] J.-H. Lee, Y.-S. Kim, K. Constant, K.-M. Ho, *Adv. Mater.* **2007**, 19, 791.
- [7] P. Nagpal, S. E. Han, A. Stein, D. J. Norris, *Nano Lett.* **2008**, 8, 3238.
- [8] X. L. Liu, T. Tyler, T. Starr, A. F. Starr, N. M. Jokerst, W. J. Padilla, *Phys. Rev. Lett.* **2011**, 107, 045901.
- [9] J. A. Mason, S. Smith, D. Wasserman, *Appl. Phys. Lett.* **2011**, 98, 241105.
- [10] J. J. Greffet, R. Carminati, K. Joulain, J. P. Mulet, S. P. Mainguy, Y. Chen, *Nature* **2002**, 416, 61.
- [11] M. Centini, A. Benedetti, M. C. Larciprete, A. Belardini, R. L. Voti, M. Bertolotti, C. Sibilia, *Phys. Rev. B* **2015**, 92, 205411.
- [12] J. H. Lee, J. C. W. Lee, W. Leung, M. Li, K. Constant, C. T. Chan, K. M. Ho, *Adv. Mater.* **2008**, 20, 3244.
- [13] J. A. Schuller, T. Taubner, M. L. Brongersma, *Nat. Photonics* **2009**, 3, 658.
- [14] M. De Zoysa, T. Asano, K. Mochizuki, A. Oskooi, T. Inoue, S. Noda, *Nat. Photonics* **2012**, 6, 535.
- [15] D. P. Sheehan, *Entropy* **2012**, 14, 1915.
- [16] N. Kumar, S. Vadera, *Aerospace Materials and Material Technologies*, Springer, Singapore, **2017**, pp. 519–537.
- [17] A. P. Raman, M. A. Anoma, L. Zhu, E. Rephaeli, S. Fan, *Nature* **2014**, 515, 540.

- [18] P. C. Hsu, A. Y. Song, P. B. Catrysse, C. Liu, Y. C. Peng, J. Xie, S. H. Fan, Y. Cui, *Science* **2016**, 353, 1019.
- [19] V. Rinnerbauer, A. Lenert, D. M. Bierman, Y. X. Yeng, W. R. Chan, R. D. Geil, J. J. Senkevich, J. D. Joannopoulos, E. N. Wang, M. Soljacic, I. Celanovic, *Adv. Energy Mater.* **2014**, 4, 1400334.
- [20] J. J. Talghader, A. S. Gawarikar, R. P. Shea, *Light: Sci. Appl.* **2012**, 1, e24.
- [21] R. Stanley, *Nat. Photonics* **2012**, 6, 409.
- [22] T. Inoue, M. De Zoysa, T. Asano, S. Noda, *Nat. Mater.* **2014**, 13, 928.
- [23] N. Bowden, S. Brittain, A. G. Evans, J. W. Hutchinson, G. M. Whitesides, *Nature* **1998**, 393, 146.
- [24] C. M. Stafford, C. Harrison, K. L. Beers, A. Karim, E. J. Amis, M. R. VanLandingham, H.-C. Kim, W. Volksen, R. D. Miller, E. E. Simonyi, *Nat. Mater.* **2004**, 3, 545.
- [25] C. Harrison, C. M. Stafford, W. Zhang, A. Karim, *Appl. Phys. Lett.* **2004**, 85, 4016.
- [26] A. L. Volynskii, S. Bazhenov, O. V. Lebedeva, N. F. Bakeev, *J. Mater. Sci.* **2000**, 35, 547.
- [27] F. Bartoli, R. Allen, L. Esterowitz, M. Kruer, *J. Appl. Phys.* **1974**, 45, 2150.
- [28] R. Gardon, *J. Am. Ceram. Soc.* **1956**, 39, 278.
- [29] D. P. DeWitt, G. D. Nutter, *Theory and Practice of Radiation Thermometry*, John Wiley & Sons, New York, **1988**.
- [30] Z. M. Zhang, B. K. Tsai, G. Machin, *Radiometric Temperature Measurements: II. Applications*, Vol. 43, Academic Press, Oxford, **2009**.
- [31] W. C. Tan, T. W. Preist, J. R. Sambles, N. P. Wanstall, *Phys. Rev. B* **1999**, 59, 12661.
- [32] P. Andrew, W. Barnes, *Science* **2004**, 306, 1002.
- [33] W. L. Barnes, A. Dereux, T. W. Ebbesen, *Nature* **2003**, 424, 824.
- [34] A. Giannattasio, I. R. Hooper, W. L. Barnes, *Opt. Express* **2004**, 12, 5881.
- [35] S. Wedge, W. Barnes, *Opt. Express* **2004**, 12, 3673.
- [36] T. Someya, T. Sekitani, S. Iba, Y. Kato, H. Kawaguchi, T. Sakurai, *Proc. Natl. Acad. Sci. USA* **2004**, 101, 9966.
- [37] S. H. Ahn, L. J. Guo, *Adv. Mater.* **2008**, 20, 2044.
- [38] M. M. Hossain, B. Jia, M. Gu, *Adv. Opt. Mater.* **2015**, 3, 1047.
- [39] T. D. James, P. Mulvaney, A. Roberts, *Nano Lett.* **2016**, 16, 3817.